Prediction of Unsteady Lifts of Oscillating Rectangular Cylinder at Low Reduced Velocities By Large Eddy Simulation

*Muhammad Waheed Sarwar[1], Takeshi Ishihara[2] and Yozo Fujino[3]

[1), 2), 3)] *Department of Civil Engineering, University of Tokyo, Tokyo, Japan*
[1)] *sarwar@bridge.t.u-tokyo.ac.jp*
[2)] *ishihara@bridge.t.u-tokyo.ac.jp*

ABSTRACT

Rectangular prisms of high thickness ratio experience vortex-induced vibrations at the reduced velocities near and lower than critical velocity (U_c). Being the common configuration for buildings and bridge sections, it is necessary to investigate the aerodynamic characteristics of rectangular prisms in detail. Aeroelastic instability of rectangular cylinders of infinite length and breadth-to-depth ratio ranging from B/D=2.0 to 4.0 were investigated numerically in a heaving mode by LES method under smooth flow conditions. Investigations are carried out employing forced oscillation method For B/D=2 and 4 with amplitudes of 0.1D to 0.02D respectively. In this study, attention was focused on frequency response component of unsteady lift force at low reduced velocities. The accuracy of results obtained by LES is assessed by comparing the numerical results with the experimental results from previous studies.

INTRODUCTION

Aeroelastic instabilities of rectangular prisms have received particular interest from both academic and practical, because of common use of such configurations in building and bridge industry, standpoints. Rectangular prisms have quite unique aerodynamic characteristics in the present context; the boundary layers separating from the sharp edges may remain separate or have intermittent attachment to the surface depending upon the breadth-to-depth ratio of prisms. Thus, making the whole process almost independent of Reynolds number (R_N) effects, which are otherwise prominent for a circular cylinder. A number of experimental studies conducted on this subject can be found in literature. However, numerical attempts to the prediction of such characteristics are scarce in literature.

[1)] Graduate Student   [2)] Associate Professor   [3)] Professor

Experimentally, many researchers like Washizu (1978), Nakamura (1975) etc. have investigated the aeroelastic instability of rectangular prisms under free and forced vibrations in detail. These studies evaluated the frequency response component (FRC) of the unsteady lift force coefficients because of its direct association with the onset of instability. Also the correlation between the unsteady lift force and velocity variation in the near wake were traced out. Komatsu (1980) conducted detailed investigations focusing on the pressure fluctuation over the surface and has explained the way a vortex is formed and shed into wake. On the other hand, many numerical studies have been carried out in this area but these were only limited to determination of mean drag, lift force and Strouhal number of square prisms (Hirano et al., 2000). In addition, Shimada (1999,2001) made use of k-ϵ model to investigate the aerodynamic characteristics of 2 dimensional rectangular prisms of varying width-to-breadth ratio (2.0≤B/D≥8.0). But considerable underestimation of total fluctuations in surface pressure and lift force were reported. Recently, Ishihara (2003) successfully applied LES approach to predict the aerodynamic features of 3D square prism in uniform flow with respect to various angles of attack. Thus, concluding the validity of LES method for prediction of mean aerodynamic features of square prisms. In summary, the performance of LES model to predict the aerodynamic instability needs to be investigated.

In this study, the aeroelastic instability of rectangular cylinders, with emphasis on the effects of B/D ratio on the aeroelastic phenomena, is investigated by LES approach. Basically, investigations are done at low wind speeds, to capture the vortex-induced vibrations, under forced oscillations. The results are compared with experimental results and also, examined to evaluate if this approach can be used for such predictions.

NUMERICAL APPROACH

LES turbulent model is used for this study in which small eddies are modeled whereas large eddies are directly calculated. Capability of LES model to capture turbulence characteristics that are unsteady and three dimensional in nature makes it the most suitable approaches for this study.

Governing Equations

The governing equations employed for LES are obtained by filtering the time-dependent Navier-Stokes equations as follows:

$$\frac{\partial \rho \overline{u_i}}{\partial x_i} = 0 \tag{1}$$

$$\frac{\partial}{\partial t}(\rho \overline{u_i}) + \frac{\partial}{\partial x_j}(\rho \overline{u_i u_j}) = \frac{\partial}{\partial x_j}\left(\mu \frac{\partial \overline{u_i}}{\partial x_j}\right) - \frac{\partial \overline{p}}{\partial x_i} - \frac{\partial \tau_{ij}}{\partial x_j} \tag{2}$$

where $\overline{u_j}$ and $\overline{p}$ are filtered mean velocity and filtered pressure respectively. ρ and τ_{ij} is the subgrid-scale stress defined by:

$$\tau_{ij} = \rho \overline{u_i} \overline{u_j} - \overline{u_i u_j} \tag{3}$$

The subgrid-scale stresses resulting from the filtering operation are unknown, and modeled as follows;

$$\tau_{ij} = -2\mu_t \overline{S}_{ij} + \frac{1}{3}\tau_{kk}\delta_{ij} \tag{4}$$

where μ_t is the subgrid-scale turbulent viscosity, and $\overline{S}_{ij}$ is the rate-of-strain tensor for the resolved scale defined by

$$\overline{S}_{ij} = \frac{1}{2}\left(\frac{\partial \overline{u}_i}{\partial x_j} + \frac{\partial \overline{u}_j}{\partial x_i} \right)$$

(5)

The Finite Volume Method was used for the descritization of governing equations. QUICK scheme for convective terms and the second order implicit scheme for unsteady terms were used. SIMPLEC method was used to solve the discritized equations. The oscillation of the models is achieved by using the sliding mesh technique. FLUENT, CFD software is used as solver.

Smagorinsky-Lilly model

The subgrid-scale turbulent viscosity μ_t is modeled using Smagorinsky model. In the Smagorinsky model, the eddy-viscosity is modeled as

$$\mu_t = \rho L_s^2 \left| \overline{S} \right| = \rho L_s \sqrt{2 \overline{S}_{ij} \overline{S}_{ij}}$$

(6)

where L_s is the mixing length for subgrid-scales, and defined as

$$L_s = \min(k\delta, C_s V^{\frac{1}{3}})$$

(7)

where k is the von Kármán constant, C_s is the Smagorinsky constant, δ is the distance to the closest wall, and V is the volume of the computational cell. An order of 0.1 for Cs is widely used in which normally explicit discritization schemes are used. Negative and positive numerical diffusion is generated in explicit and implicit discritization schemes respectively. Therefore, in this study smaller value of Cs, 0.032, is used based on the study in which spectrum approach was applied to a LES calculation (Ma et al. 2000).

Boundary Conditions for the LES model

If the mesh is fine enough to resolve the laminar sublayer, the wall shear stress is obtained from the laminar stress-strain relationship:

$$\frac{\overline{u}}{u_\tau} = \frac{\rho u_\tau y}{\mu}$$

(8)

If the mesh is too coarse to resolve the laminar sublayer, it is assumed that the centroid of the wall-adjacent cell falls within the logarithmic region of boundary layer, and the law-of-the-wall is employed:

$$\frac{\overline{u}}{u\tau_\tau} = \frac{1}{k} \ln E\left(\frac{\rho u_\tau y}{\mu} \right)$$

(9)

Where u_τ is the friction velocity, k (von Kármán) constant is 0.418 and constant E is 9.793.

Sliding mesh theory

In the sliding mesh, two or more cell zones are used. Each cell zone is bounded by at least one "interface zone" where it meets the opposing cell zone. The interface zone of adjacent cell zones

is associated with one another to form a "grid interface". The two cell zones will, then, move relative to each other along the grid interface. In doing so, the grid faces do not need to be aligned on the grid interface. This situation requires a means of computing the flux across the nonconformal interface zones of each grid interface.

To compute the interface flux, the intersection between the interface zones is determined at each new time step. The resulting intersection produces one interior zone and one or more periodic zones/a pair of wall zones. The resultant interior zone corresponds to where the two interface zones overlap; the resultant periodic/wall zone corresponds to where they do not. The number of faces in these intersection zones will vary as the interface zones move relative to one another. Principally, fluxes across the grid interface are computed using the faces resulting from the intersection of the two interface zones, rather than from the interface zone faces themselves.

Description of grid domain

In this study, two width to breadth ratios B/D=2.0 and 4.0 are used, because these two cases are typical of fully separated and intermittently reattached type of sections. Fig 1 shows computational domain used in this study along with the static zone, moving zone and interface zones. The dimensions of each prism model are shown in table 1. The corners are considered rounded with radius to depth ratio (r/D) of 0.01 as shown in Fig 2. The width and depth of domain are 100D and 60D respectively. Inflow wind-velocity "U" is kept 20 m/s to avoid any additional phenomenon, if any, arising with change in R_N. The maximum intensity of turbulence is of the order of 0.001% at the inlet boundary. Throughout our study, the angle of attack, angle between the direction of width B and that of the uniform flow, was kept zero.
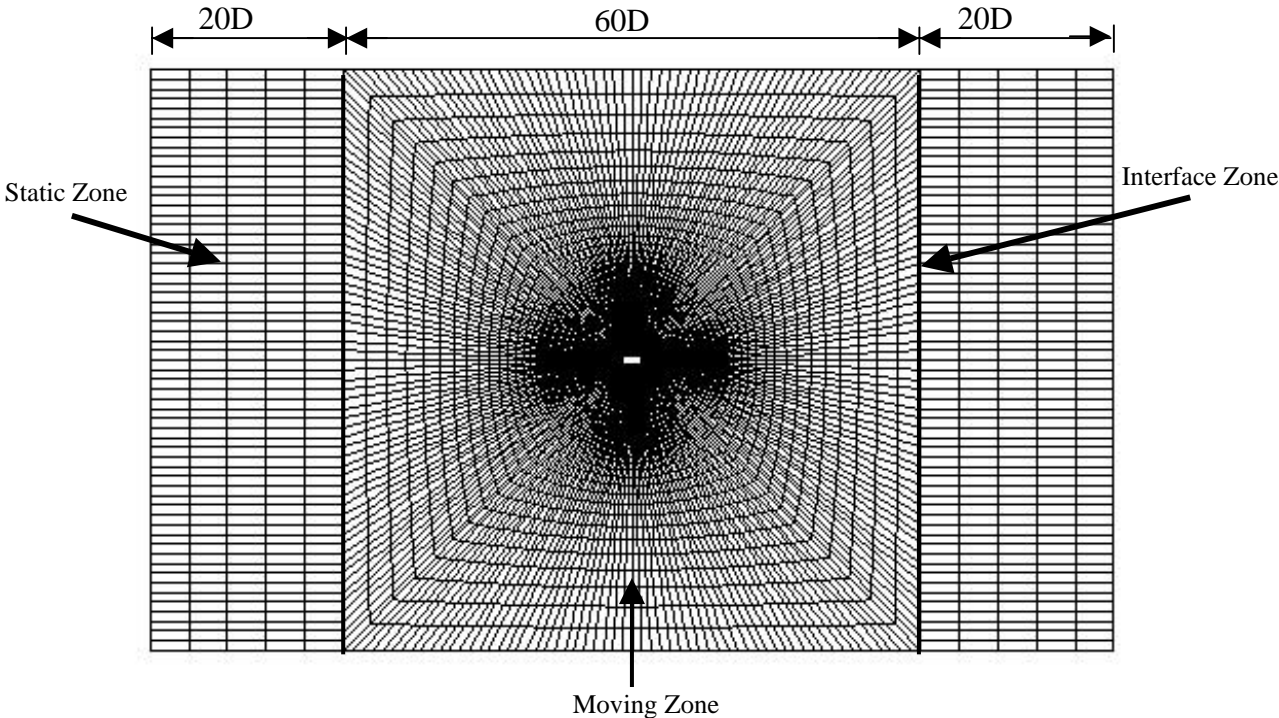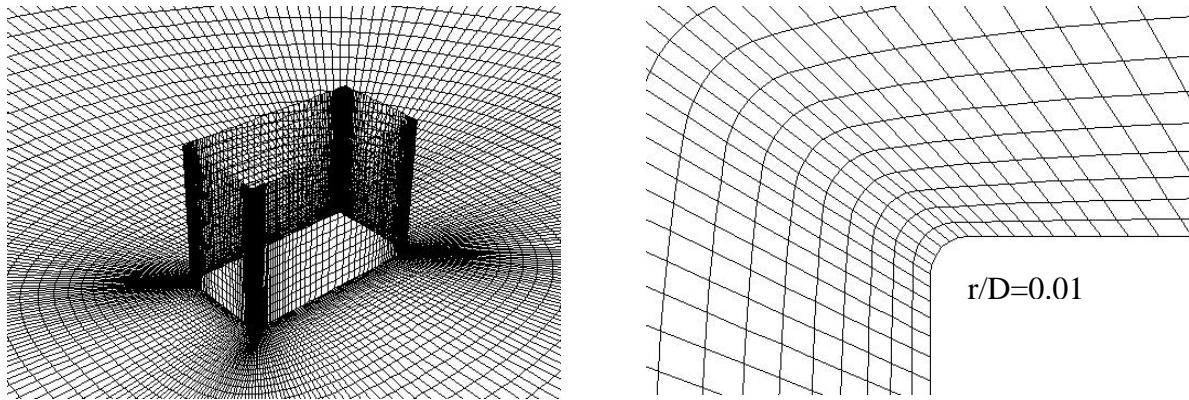

Figure 1. Computational Domain of Rectangular Prism

(a) Grid near the Rectangular Prism   (b) Grid at the corner

Figure 2. Details of grid near and at the corner of the rectangular prism

Models are subjected to forced oscillations in the heaving mode only. A sliding mesh technique with non-periodic grid interface is employed to allow the forced oscillations of the rectangular prism in y-direction. The boundary conditions for the wall zones produced from the moving interface zones are set to be velocity-inlet as per required by Fluent. Outflow boundary condition was used at outlet boundary. Symmetry condition was used for top and bottom surface of the domain. The number of mesh used for edges of B/D=2.0 and 4.0 are 70 x 50 and 80 x 40 respectively. Smaller meshes were generated at each edge corner to avoid singularity of the solutions. And equally distributed 15 meshes were used in span wise direction. Total number of mesh used for model 1 and 2 are 293,000 and 320,000 respectively. For each model, 10 cases with reduced velocity ranging from 3 to 20 were chosen for the calculation purposes.

Table 1. Model Dimensions and Analysis Parameters

Models	I	II
D (cm)	1	1
B (cm)	2	4
Z (cm)	1.5	1.5
R_N	13,000	
Cs	0.032	
Span wise number of meshes	15	
Total no of meshes	293,000	320,000

Forced oscillations and frequency response of unsteady lift force

The models were placed in 3D flow in direction of the prism width and subjected to a forced sinusoidal oscillation,

$$h(t) = h_o \cos\omega t \qquad (10)$$

where h_o is amplitude of oscillation and ω is the frequency of oscillation. The sliding mesh is subjected to transverse displacement obtained by the above expression. And the resulting aerodynamic force L(t) was measured, L(t) and h(t) are considered positive along the

positive z-direction. During this study, we chose the amplitude of oscillation h_o as a variable parameter as follows: for model 1(B/D=2), h_o=0.1D and for model 2 (B/D=4), h_o=0.02D. The reason behind choosing amplitude h_o=0.02D of model 2 will be described in later section. The corresponding reduced wind velocity (Ur=U/f.h) was in the range of 3-20 where "f " represents the frequency of forcing oscillation.

The frequency response part is expressed as follows:

$$C_L(t) = C_{Lo}\cos(\omega t + \beta) \tag{11}$$

where C_{Lo} is amplitude of the lift coefficient force coefficient and β is the phase difference between the exciting force and lift force acting on the surfaces. These can be obtained from lift force history from numerical calculations as explained below:

$$C_{Lo} = \sqrt{(a_m^2 + b_m^2)} \quad \text{and} \quad \tan(\beta) = -b_m/a_m \tag{12a}$$

$$[a_m, b_m] = \frac{1}{T} \int_{-T}^{T} C_L(t)[\cos \omega t, \sin \omega t] dt \tag{12b}$$

And the real and imaginary part of the lift coefficients is determined using following relations:

$$C_{LR} = C_{Lo}\cos(\beta) \quad , \quad C_{LI} = C_{Lo}\sin(\beta) \tag{13}$$

Details on this subject could be found in Washizu et al. (1978). It is worth mentioning here that the system becomes unstable at a condition when $C_{LI} \geq 0$ indicating the negative aerodynamic damping region leading to self excited vibration of the system.

RESULTS AND DISCUSION

This section includes the results of frequency response component of the unsteady lift, obtained from numerical simulation, acting on the oscillating prisms. The characteristic of wake flow is examined by evaluating the phase difference between the wake velocity and forcing oscillation. Also, the variation of pressure around the prisms during oscillation is visualized and vortex formation and shedding into wake is discussed.
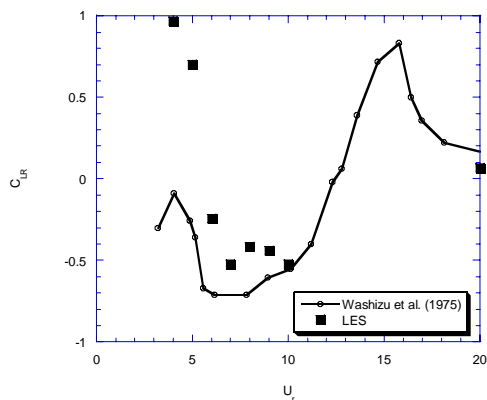
Frequency response part for model 1 with B/D=2

Fig 3 shows the characteristic frequency response of model 1 subjected to amplitude of 0.1D. The ordinates are dimension-less lift force coefficient (C_L), the phase angle β, the real part C_{LR} and imaginary part C_{LI}, whereas the abscissa is the reduced wind velocity (Ur=U/f.h).

Fig 3(b) shows the variation of the imaginary part of lift coefficient that corresponds to the instability due to negative aerodynamic damping. C_{LI} changes from negative to positive at low reduced velocity of 5 and then again becomes negative till reduced velocity of 20 is reached. Thus, indicating the presence of self excited vibration at about Ur=5, called vortex induced vibrations and that of Ur≥20 leading to the galloping phenomenon. This is the same behavior that is observed in the experimental results of previous studies. Comparison of present results and previous experimental results show good agreement regarding the onset of instability at low reduced velocities. However, the predicted values of C_{LR} differs from the experimental values at reduced velocities lower than 6.

Fig 3(c) shows the phase angle of the lift force to the excitation force. An abrupt phase change with the reduced velocity is well capturd by numerical simulation, and this prediction

agrees well with what is reported by previous experiments. Fig 3(d) shows change in dimensionless amplitude with increase in the reduced velocity. A good agreement can be observed among the experimental and numerical results.
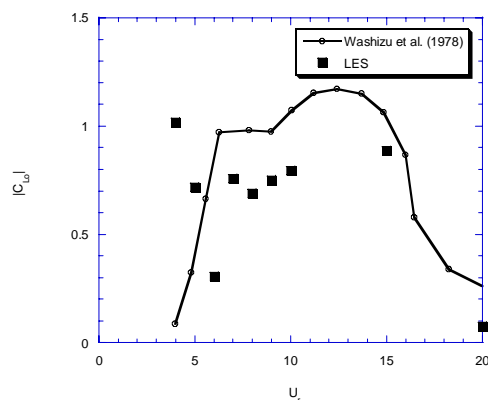

(a) Real Part of Complex Amplitude of Unsteady Lift Force Coefficient Vs Reduced Velocity
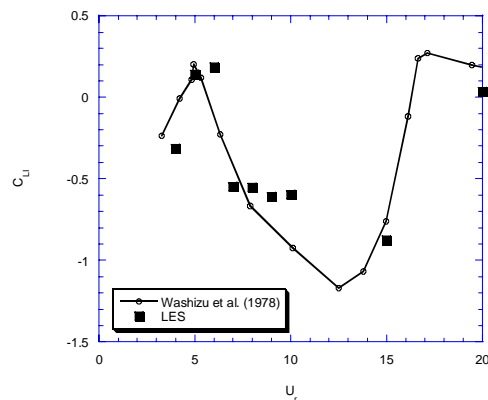
(b) Imag. Part of Complex Amplitude of Unsteady Lift Force Coefficient Vs Reduced Velocity
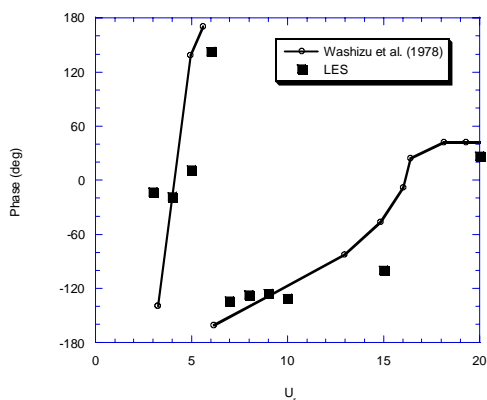
(c) Phase Angle Vs Reduced Velocity

(d) Absolute Value Vs Reduced Velocity

Figure 3. Real Part, Imaginary Part, Phase Angle and Absolute Value of Unsteady Lift Force Coefficient Vs Reduced Velocity for Model 1 (B/D=2) with amplitude 0.1D

Frequency response part for model 2 with B/D=4

Fig 4 shows the characteristic frequency response of model 2 subjected to amplitude of 0.02D. The ordinates are dimensionless lift force coefficient (C_L), the phase angle β, the real part C_{LR} and imaginary part C_{LI}, whereas the abscissa is the reduced wind velocity (U_r=U/f.h).

In case B/D=4, experimental results show that only for small amplitude, C_{LI} becomes positive in the vicinity of the resonance speed (Washizu et al. 1978). Whereas at large amplitudes, C_{LI} remain negative through out experimental range of reduced velocity, i.e., system did not show any signs of instability at large amplitude of vibration. Therefore, authors chose small amplitude of 0.02D in order to check capability of the method used to predict the instability of system.

Fig 4(b) shows the variation of the imaginary part of lift coefficient that corresponds to the instability due to the negative damping. C_{LI} become from negative to positive at low reduced

(a) Real Part of Complex Amplitude of Unsteady Lift Force Coefficient Vs Reduced Velocity

(b) Imag. Part of Complex Amplitude of Unsteady Lift Force Coefficient Vs Reduced Velocity

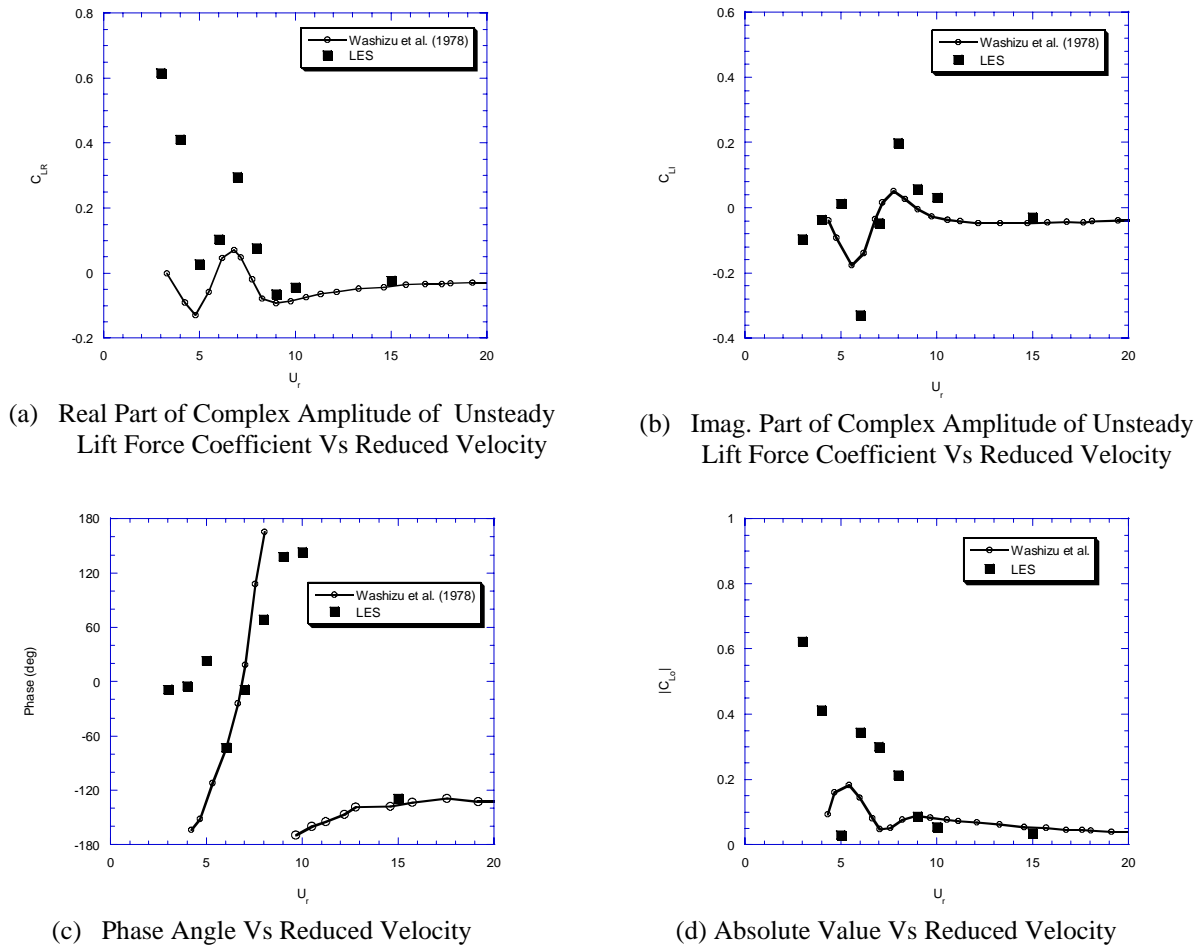(c) Phase Angle Vs Reduced Velocity

(d) Absolute Value Vs Reduced Velocity

Figure 4. Real Part, Imaginary Part, Phase Angle and Absolute Value of Unsteady Lift Force Coefficient Vs Reduced Velocity for Model 2 (B/D=4) with amplitude 0.02D

velocity of 8 and then again becomes negative for the higher values of reduced velocity. Thus, indicating the presence of self excited vibration at about Ur=8, called vortex induced vibrations. Also calculation shows the change in sign of C_{LI} at Ur=5 which is in accordance with the pattern observed from experimental results. The tendency of C_{LI} to remain negative represents absence of galloping in this case that is what can be seen from experimental findings. Comparison of present results and previous experimental results show good agreement regarding the onset of instability at low reduced velocities. However, the calculated values of C_{LR} differs from the experimental values at reduced velocities lower than 6.

Fig 4(d) shows change in dimensionless amplitude with the increase in the reduced velocity. A good agreement can be observed among the experimental and numerical results.

Frequency response component of flow velocity

Figure 5 shows the change in phase angles of the frequency response component of the wake flow velocity $U_w(t)$ with change in reduced velocity. The wake flow velocity of forced vibrations was measured at the points, which are shown in the respect case, but the points were

kept stationary to match the experimental procedure. The procedure used to calculate the frequency response is similar to that of used for the unsteady lift force coefficient.

From these figures, a tendency of sharp increase in phase angle at the low reduced velocities can be observed. However, less change in phase angle is obtained with increase in reduced velocity. At low reduced velocity, fairly close resemblance can be seen between phase angles of the lift coefficient and that of wake flow velocity. Also, comparison of numerical results with experimental ones reported by Nakamura et al. (1975) shows good agreement.

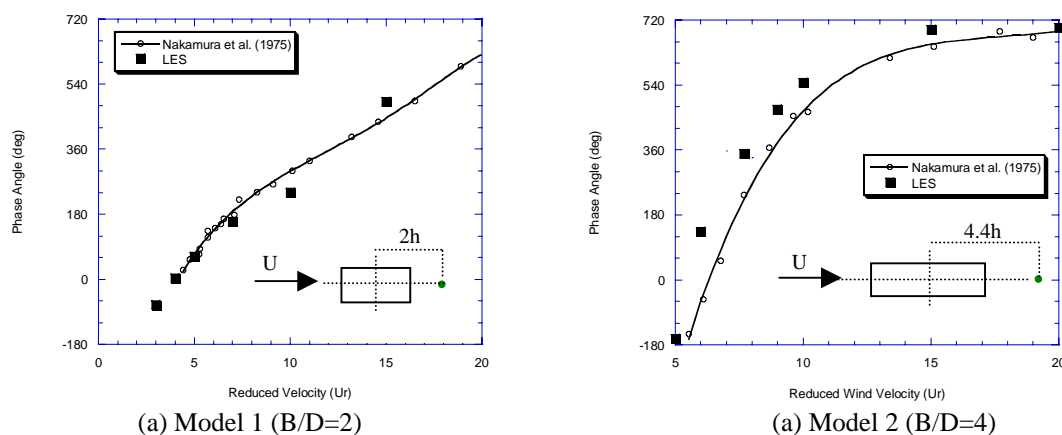(a) Model 1 (B/D=2)   (a) Model 2 (B/D=4)

Figure 5. Phase Angle of Frequency Response Component of Wake Flow Velocity Versus Reduced Wind Velocity

Variation of flow and pressure distribution around oscillating prisms

To understand the flow characteristics around the oscillating prisms, the pressure fluctuations around the rectangular prisms are investigated. Figures (6) and (7) show the instantaneous flow-patterns around the cylinders during one cycle of forced oscillation. The prisms with B/d=2 and 4 are subjected to forced sinusoidal oscillations with amplitudes 0.1D and 0.01D respectively. The positions of oscillating prism for the corresponding pressure distributions are also shown in the respective figures.

Flow separates at the leading edge of both oscillating prisms and then reattach to the surface before reaching the rear edge. From the figures, a vortex formation just behind the leading edge can be observed that then travels down the leeward side along the surface. A negative pressure is produced on the upper surface just after the maximum amplitude of oscillation is reached. This gives rise to a vortex formation by concentration of large negative pressure over limited range of the surface during the downward motion of the prism. This concentration reach to maximum value by the time lowest position during oscillation is achieved and this vortex starts moving towards rear edge due to dragging action of the mean flow along the surface of prism during the upward oscillation. And departure of vortex from the upper surface occurs when prism reaches the uppermost position during the oscillation. Same behavior is observed over the lower surface too.

The visualization of flow pattern shows that vortex keeps on growing during the half cycle from one extreme position to other one, and travels to rear edge resulting in shedding into
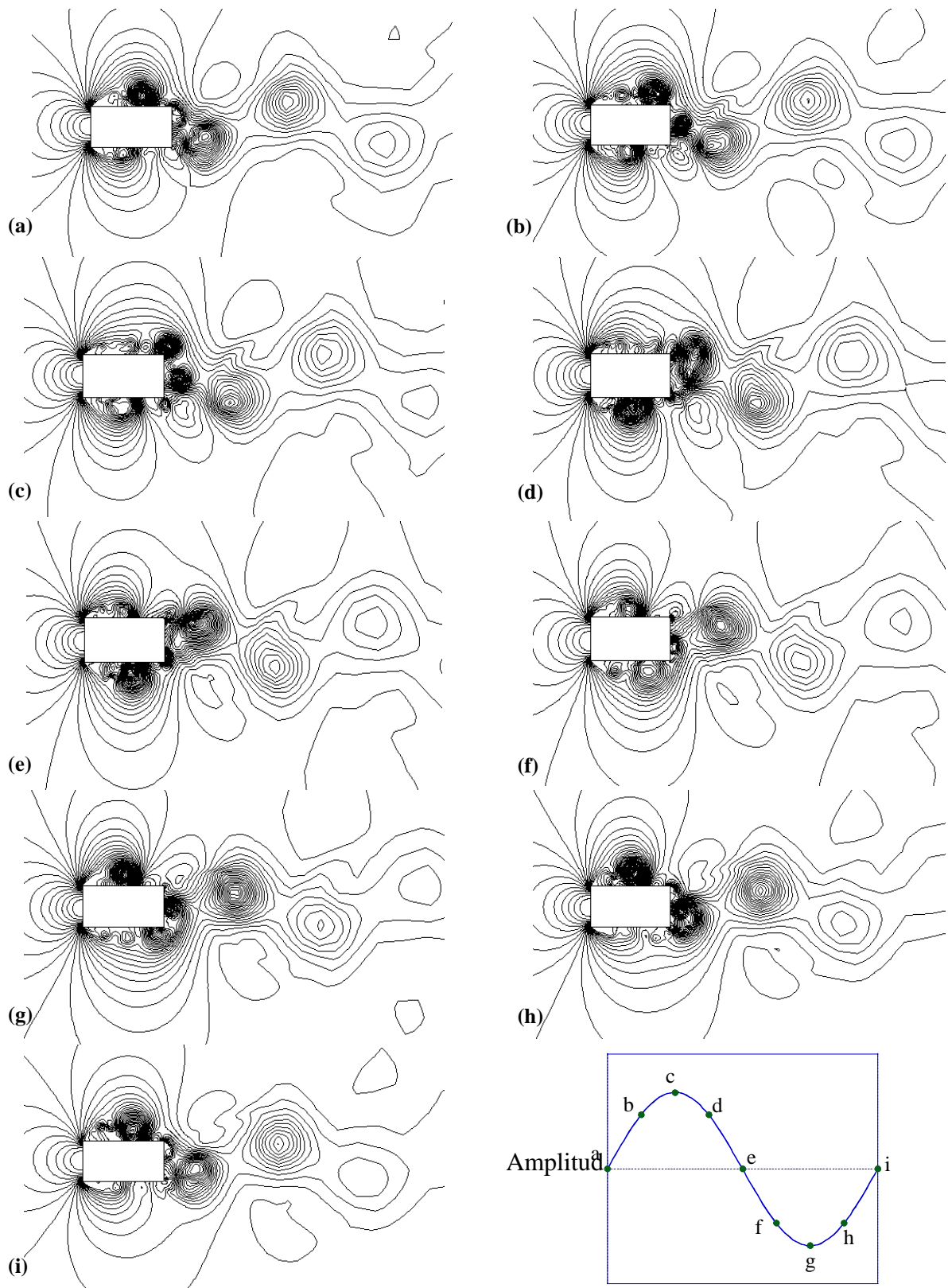
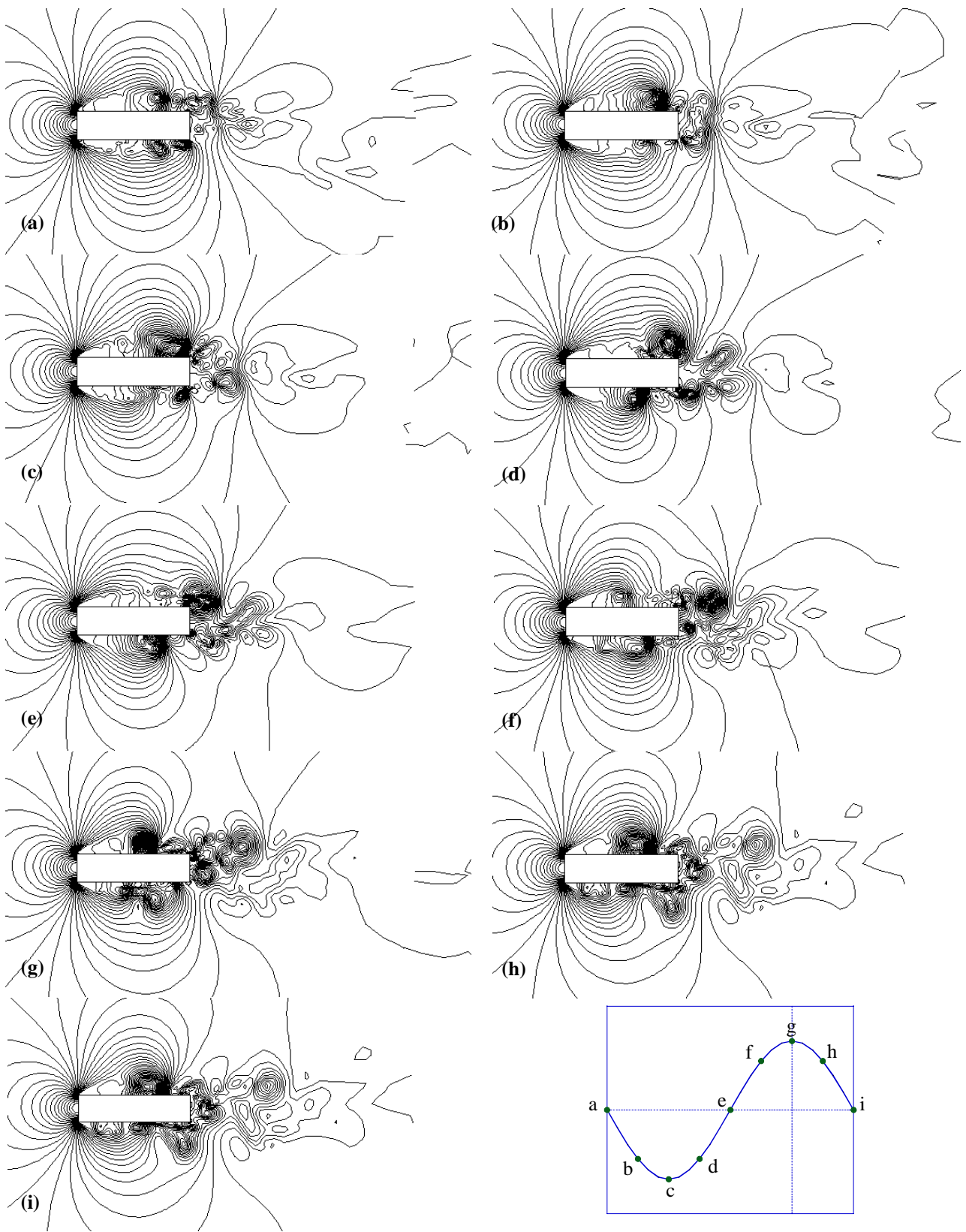Figure 6. Instantaneous flow patterns during oscillation of rectangular prism (B/D=2) at Ur=6.

Figure7. Instantaneous flow patterns during oscillation of rectangular prism (B/D=4) at Ur=8.

the wake on the way back to the original extreme position. Also, it can be seen that at the time the negative pressure concentrates leading to vortex formation on the upper surface, vortex of lower edge is departing to the wake that results into relatively less negative pressure on lower surface. As a result, prism is subjected to an upward lift that is in accordance with the upward motion of the prism and vice versa. This interaction between the lift force and the prism movement is repeated in each oscillation. Therefore, it can be concluded that the prism is subjected to an exciting force whose frequency is equal to that of the oscillating prism. The formation of vortex on the surface is subjecting the cylinder to relatively large lift force as compared to case where only Karman vortex is present, i.e., for static cases. This simulated behavior agrees with the explanation given by Komatsu et al. (1980) based on the experimental results.

CONCLUSIONS

The aerodynamic instabilities of rectangular prisms having different side ratios of 2 and 4, in heaving mode under uniform flow conditions were investigated using LES turbulence model and then compared with experiments. The study has been conducted by employing forced oscillation method. Following are the conclusion drawn from this study:

1) The resonance characteristics of rectangular prisms under external forcing oscillations are pursued. The possibility of occurrence of vortex excitation and galloping for B/D=2 is well predicted. In addition, absence of transverse galloping for B/D=4 is also indicated by the numerical work. An abrupt phase change in lift force leading to the generation of negative aerodynamic damping is well captured and the estimated values are well within the experimental data.
2) The phase angle of wake velocity shows sharp change at low reduced velocities and rather, mild change is observed at higher velocities. Though, some shift is observed among experimental and numerical values for rectangular prism with B/D=4, overall pattern is found in good agreement qualitatively.
3) The mechanism of vortex formation and shedding into wake for the cases where separation points are on the leading edge is discussed. The numerical produces clear image of this phenomenon which otherwise is not easier to get with smoke tests.
4) The region of very low reduced velocities (Ur=3~5) shows much difference from the experimental results. Since wake effect may influence the flow strongly for such reduced velocities, further numerical investigations must be carried out in this region.

This numerical approach successfully predicts the occurrence of aerodynamic instability of rectangular prisms with different width-to-depth ratios. In conclusion, this approach can be applied to cases where vortex excitation is expected and further studies for the complex sections used in real world structures are considered necessary.

REFERENCES

Hirano, H., Maruoka, A. and Watanabe, S., (2000)"Calculation of aerodynamic properties of rectangular cylinder with slenderness ration of 2:1 under various angle of attack", *Journal of Structural Engineering*, JSCE, Vol. 48A, 971-978

Ishihara, T. and Oka, S., (2003)"Numerical study of aerodynamic force and surface pressure of square prism in a uniform flow", Proceedings of Eleventh International Conference on *Wind*, Texas Tech University.

Komatsu, S. and Kobayashi, H. (1980) "Vortex-induced Oscillation of bluff cylinders", *Journal of Wind Engineering and Industrial Aerodynamics*, 6,335-362

Morgenthal, G. (2002) "Aerodynamic Analysis of Structures Using High-resolution Vortex Particle Methods", PhD Thesis, Department of Engineering, University of Cambridge

Nakamura, Y. and Mizota, T. (1975) "Unsteady lifts and wakes of oscillating rectangular prisms". *Journal of the Engineering Mechanics Division*, Dec 1975, 885-871

Shimada, K., Ishihara, T., (1999) "Prediction of aeroelastic vibration of rectangular cylinders by K-ϵ model", *Journal of Aerospace Engineering*, 12(4), 122-135

Shimada, K., Ishihara, T., (2001) "Application of modified K-ϵ model to the prediction of aerodynamic characteristics of rectangular cross-section cylinders", *Journal of Fluids and Structures*, 16(4), 465-485

Washizu, k., Ohya, A., Otsuki, Y. and Fuji, K. (1978)"Aeroelastic instability of rectangular cylinders in a heaving mode", *J. of Sound and Vibration*, 59(2), 195-210